Macromolecules
ARTICLE

Macromolecules **2010**, *43*, 1455–1466 **1455**
DOI: 10.1021/ma902502f

Channel Clathrate of Syndiotactic Polystyrene with *p*-nitroaniline

Oreste Tarallo,* Maria Maddalena Schiavone, and Vittorio Petraccone

Dipartimento di Chimica "Paolo Corradini", Università degli Studi di Napoli Federico II, Complesso di Monte S. Angelo, via Cintia, 80126 Napoli, Italy

Christophe Daniel, Paola Rizzo, and Gaetano Guerra

Dipartimento di Chimica, Università degli Studi di Salerno, via Ponte Don Melillo, 84084 Fisciano (SA), Italy

Received November 11, 2009; Revised Manuscript Received December 16, 2009

ABSTRACT: The detailed description of the crystalline structure of a channel type ε clathrate cocrystal of syndiotactic polystyrene (s-PS) is presented here for the first time. The proposed structure is based on X-ray diffraction experiments, molecular mechanics calculations and infrared measurements. The guest molecule is *p*-nitroaniline (NA), a highly polar molecule which makes its cocrystals possibly suitable for nonlinear optical and piezo-electric materials. X-ray data are interpretable in terms of the orthorhombic unit cell (a = 1.62 nm, b = 2.20 nm and c = 0.79 nm) and the space group *Pbcn* already proposed for the nanoporous ε form indicating that the crystal packing of the chains in the clathrate form remains substantially unaltered in respect to that of the nanoporous form. NA guest molecules are placed in the channels delimited by the chains with a high degree of freedom along the channel axis but with their dipole almost parallel to the chain axis and forming with their main molecular plane an angle of nearly ±20° with the *bc* plane. Moreover, in each channel guests are stacked all with a same relative dipole orientation and are not uniformly distributed but arranged in "couples", in which molecules are linked by hydrogen bonds. A quantitative analysis of the crystal structure of the nanoporous s-PS ε form is also presented.

1. Introduction

Syndiotactic polystyrene (s-PS) presents a very complex polymorphic behavior including five different crystalline phases.[1] Moreover, s-PS is able to form different kinds of cocrystalline phases with a large number of guest molecules.[2−4] All of these exhibit an s(2/1)2 helical polymer conformation, with a repetition period of nearly 0.78 nm.

Most s-PS cocrystals[2,3] are characterized by the *ac* layers of close-packed alternated enantiomorphous helices, typical of the nanoporous monoclinic δ form.[5] These can be defined δ *cocrystals* and can be divided in two classes: δ *clathrates*, with guest molecules imprisoned into isolated cavities (cooperatively generated by two enantiomorphous helices of two adjacent *ac* layers) and generally characterized by a maximum guest/monomer-unit molar ratio of 1/4,[2] and δ *intercalates* (or simply intercalates), characterized by the *ac* layers of helices alternated to layers of contiguous guest molecules[3,6] and generally by a maximum guest/monomer-unit molar ratio of 1/2.[3]

Recently, a third class of s-PS cocrystals has been obtained by guest sorption in the nanoporous orthorhombic ε phase of s-PS.[4b] In these cocrystals, defined as ε *clathrates*, guest molecules are imprisoned into channels passing the unit cells of the ε form from side to side along the *c* direction.[4] In the ε clathrates also guest molecules being longer than the repetition period of the helices can be hosted.[4]

This contribution presents, for the first time, the detailed description of the crystalline structure of a channel type ε clathrate cocrystal of s-PS. The proposed structure is based on X-ray diffraction experiments of unoriented and oriented samples, molecular mechanics calculations and infrared measurements. To support this structural study we have also performed a more quantitative analysis of the crystal structure of the nanoporous s-PS ε form, already presented by some of us in a recent paper in its most relevant aspects.[4b]

The relevance of this structural study is also associated with the high polarity of the *p*-nitroaniline (NA) guest molecule[4a] ($\mu \approx 6.2$ D), which is of type A−π−D (where A and D are electron acceptor and donor groups, respectively) and hence possibly suitable for materials with nonlinear optical and piezoelectric properties. It is worth noting that NA molecules and analogous A−π−D molecules have been also included in channels of inorganic (zeolites)[7a] or of organic[7b,c] host crystalline structures, leading to crystals showing pyroelectric and second-harmonic generation effects.

As for possible practical applications, the main advantage of the polymer cocrystals, with respect the inorganic and organic cocrystals, is their easy production in the form of films of any thickness, also exhibiting high degree of orientation of the cocrystalline phase. In particular, as for δ cocrystalline phases, the possibility to obtain three different kinds of uniplanar orientations,[8] beside the usual axial orientation,[9] and hence long-range 3-D orientational order of active guest molecules,[10] has been deeply studied. For the nanoporous ε phase, it has been recently described the achievement of three different kinds of uniplanar orientations (exhibiting the *a*, *b*, and *c* crystalline axes preferentially perpendicular to the film plane), which correspond to three different orientations of the empty channel with respect to the film plane.[11] This polymer-host orientation control and the knowledge of the crystalline structure of the ε-clathrate with NA (main objective of this paper) is expected to give a control of the 3-D orientational order of the polar guest molecules, also at macroscopic level. In this respect, a possible aim is the

*Corresponding author. Telephone: +39-081-674443. Fax: +39-081-674090. E-mail: oreste.tarallo@unina.it.

Published on Web 01/08/2010

achievement of guest dipole orientation nearly perpendicular to the film plane, being most suitable for poling processes.

2. Experimental Part

2.1. Materials. The s-PS used in this study was manufactured by Dow Chemical Company under the trademark Questra 101. The ^{13}C nuclear magnetic resonance characterization showed that the content of syndiotactic triads was over 98%. The weight-average molar mass obtained by gel permeation chromatography (GPC) in trichlorobenzene at 135 °C was found to be $M_w = 3.2 \times 10^5$ with the dispersity index $M_w/M_n = 3.9$.

Chloroform, *p*-nitroaniline, carbon disulfide, and toluene were purchased from Aldrich and used without any further purification.

2.2. Preparation of the Samples. s-PS ε form samples are generally obtained by exposure of samples in the γ form to liquid $CHCl_3$ at room temperature and its subsequent removal by immersion in acetonitrile or with supercritical carbon dioxide.[4] To our knowledge these samples always present a minor portion of the γ form while being completely free of the δ form.

The oriented sample used in the present paper for the reexamination of the ε form was prepared starting from an oriented film in the *trans*-planar mesomorphic form[12] dipped (for 24 h) in liquid chloroform at room temperature,[12d] keeping the ends of the specimen fixed. The $CHCl_3$ removal was then effected by immersion in acetonitrile for 30 min. The thus obtained ε form sample presents only a minor content of the γ form.

s-PS mesomorphic film was obtained by uniaxially stretching of an amorphous film at 300%, at strain rate of 0.1 s^{-1}, in the temperature range 105−110 °C with a dynamometer INSTRON 4301. Amorphous films, 150−200 μm thick, were obtained by extrusion of the melt with an extrusion head of 200 mm ×0.5 mm.

Oriented films in the cocrystalline form containing *p*-nitroaniline were obtained by immersion (for 36−48 h) of films in the crystalline ε form in a saturated solution of *p*-nitroaniline in acetonitrile keeping the ends of the specimen fixed. The nanoporous ε form used was obtained by room temperature treatments with liquid chloroform of oriented γ form films and subsequent removal of $CHCl_3$ with acetonitrile. Films in the crystalline γ form were obtained by annealing at 135 °C for 24 h of films in the δ form that, in turn, were obtained by room temperature CS_2 vapor treatments for 48 h of uniaxially stretched mesomorphic films, followed by thermal treatments at 40 °C under vacuum for 48 h.

Unoriented nanoporous ε form samples were obtained by dipping (for 24 h) at room temperature in liquid $CHCl_3$ unoriented samples in the γ form and then by its removal by acetonitrile treatments for 6 h. Unoriented s-PS γ form samples were obtained by annealing at 135 °C (for 8 h) unoriented s-PS/toluene δ clathrate samples obtained in turn from the dissolution in toluene of the commercial pellets for 4 h.

Unoriented samples of the ε clathrate with *p*-nitroaniline were obtained by immersion of powders in the crystalline ε form in a saturated solution of *p*-nitroaniline in acetonitrile for 10−12 days.

The overall amount of the NA guest molecules in the semicrystalline ε/NA samples has been evaluated by measurement of FTIR absorbances of the NA peak at 1119 cm^{-1} by using a calibration obtained from a thermogravimety analysis performed with a TG 209 F1 from Netzsch.

2.3. FTIR Measurements. Infrared spectra were obtained at a resolution of 2.0 cm^{-1} with Bruker spectrometers (Vertex70 and Tensor27) equipped with deuterated triglycine sulfate (DTGS) detector and a KBr beam splitter. The frequency scale was internally calibrated to 0.01 cm^{-1} using a He−Ne laser. A total of 32 scans were signal averaged to reduce the noise.

The degree of crystallinity was evaluated by the FTIR procedure described in ref 13 and all the considered samples are semicrystalline with a degree of crystallinity in the range 30−40%.

The relative amount of NA molecules included in the amorphous phase of δ/NA (or ε/NA) cocrystalline samples was evaluated from FTIR spectra from the symmetric N−H stretching peak ($\nu_s(NH_2)$) using a δ/NA (or ε/NA) sample with all NA molecules being guest of the cocrystalline phase (i.e., after complete acetone removal) for the spectral subtraction.

The fraction of NA molecules included in the amorphous phase ($X_{NA,am}$) is given by:

$$X_{NA,am} = \frac{A_{total}(\nu_s(NH_2)) - KA_{NA,c}(\nu_s(NH_2))}{A_{total}(\nu_s(NH_2))}$$

where $A_{total}(\nu_s(NH_2))$ is the total absorbance area of the $\nu_s(NH_2)$ peak of the analyzed sample, $A_{NA,c}(\nu_s(NH_2))$ is the absorbance area of the $\nu_s(NH_2)$ peak corresponding to the δ/NA (or ε/NA) sample with all NA molecules being guest of the cocrystalline phase (i.e $\nu_s(NH_2)$ peak located at 3400 cm^{-1}), and K is a parameter evaluated during spectral subtraction in order to reduce to zero (to the baseline) the absorbance of the sample at 3400 cm^{-1}.

Polarized infrared spectra were obtained using a KRS-5 polarizer from Specac. As usual, for each infrared peak of axially oriented samples, an order parameter S can be defined as the ratio:

$$S = (R-1)/(R+2) \quad (1)$$

where $R = A_{\parallel}/A_{\perp}$ is the dichroic ratio, $A_{\parallel}$ and $A_{\perp}$ being the measured absorbance for electric vectors parallel and perpendicular to the draw direction, respectively. The orientation factor relative to the helical chains of the host polymer phase ($f_{c,IR}$) has been evaluated by the dichroic ratio of the 571 cm^{-1} infrared band.[14]

2.4. X-ray Diffraction. The X-ray fiber diffraction patterns of oriented samples were obtained on a BAS-MS imaging plate (FUJIFILM) with a cylindrical camera (radius 57.3 mm, Ni-filtered Cu−Kα radiation monochromatized with a graphite crystal) and processed with a digital scanner (FUJI-BAS 1800). Calculated intensities were obtained as $I_c = F_c^2 M_i B L p$ where F_c is the calculated structure factor, M_i is the multiplicity, B is a thermal factor ($B = 8$ Å^2) and Lp is the Lorentz−polarization factor for X-ray fiber diffraction:

$$L_p = \frac{\left(\frac{0.5(\cos^2 2\theta + \cos^2 2\theta_M)}{1+\cos^2 2\theta_M} + \frac{0.5(1+\cos 2\theta_M \cos^2 2\theta)}{1+\cos 2\theta_M}\right)}{(\sin^2 2\theta - \zeta^2)^{1/2}} \quad (2)$$

with $2\theta_M = 26.6°$ the inclination angle of the monochromator and $\zeta = \lambda(l/c)$, l and c being the order of the layer line and the chain axis periodicity, respectively, and λ the wavelength of the used radiation (1.5418 Å). Calculated structure factors were obtained as $F_c = (\sum |F_i|^2 M_i)^{1/2}$, where the summation is taken over all reflections included in the 2θ range of the corresponding spot observed in the X-ray fiber diffraction pattern. Atomic scattering factors from ref 15 were used. The observed intensities I_{obsd} were evaluated integrating the crystalline peaks observed in the X-ray diffraction profiles, read along different layer lines, after the subtraction of the background, amorphous and γ form contributions. Owing to the different shapes of the reflections on the equator and on the first and second layer lines, due to the different dimensions of the lamellar crystals in the direction perpendicular and parallel to the chain axis, different factors were used to scale the observed and calculated structure factors

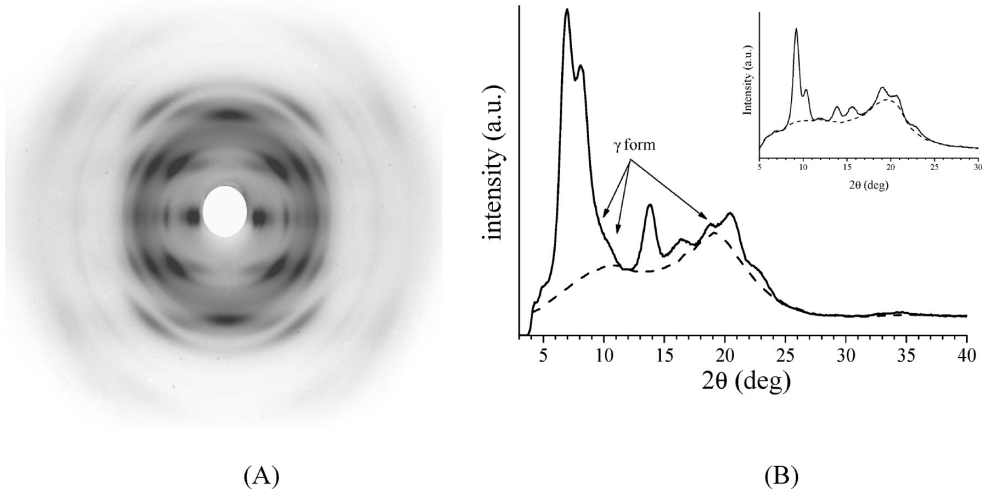

Figure 1. (A) X-ray diffraction pattern of an oriented sample of the nanoporous ε form of s-PS. Fiber axis is vertical. In the corresponding equatorial intensity profile, (B) the arrows indicate the positions of the reflections due to a small amount of γ form. The inset shows the typical equatorial intensity profile of an oriented γ form sample. Amorphous and background contributions are indicated with dashed lines.

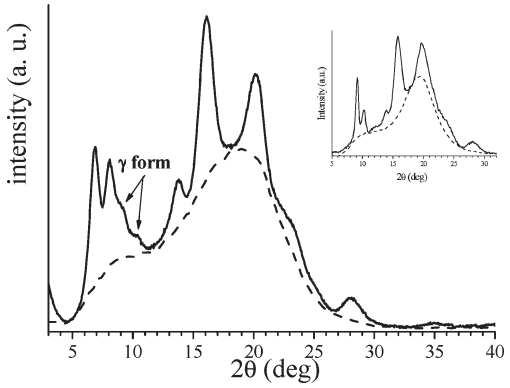

Figure 2. X-ray diffraction pattern of an unoriented sample of the nanoporous ε form of s-PS. The arrows indicate the position of the reflections due to a small amount of γ form. The inset shows the typical intensity profile of an unoriented γ form sample. Amorphous and background contributions are indicated with dashed lines.

on the diverse layer lines. The discrepancy factor R has been evaluated as $R = \Sigma|F_{obsd} - F_{calcd}|/\Sigma F_{obsd}$ taking into account only the observed reflections.

The contribution to the diffraction intensity of the γ form has been subtracted in the X-ray diffraction profiles of the oriented sample of ε form by a deconvolution procedure performed with the Peak Fitting module of Origin 7.0 by OriginLab Corporation. The peaks have been considered as Gaussians of fixed full width at half-maximum height. The positions and the intensity ratios between the diffraction peaks of γ form have been imposed according to the experimental profile of a pure oriented γ form sample.

Wide-angle X-ray diffraction patterns of unoriented samples were obtained with nickel-filtered Cu Kα radiation with an automatic Philips powder diffractometer operating in the $\theta/2\theta$ Bragg−Brentano geometry using specimen holders 2 mm thick.

Calculated X-ray powder diffraction pattern were obtained with the *Diffraction-Crystal* module of the software package *Cerius*[2] (version 4.2 by *Accelrys Inc.*) using an isotropic thermal factor (B = 8 Å^2). A Gaussian profile function having a half-height width regulated by the average crystallite size along a, b, and c axes (L_a, L_b and L_c, respectively) was used. A good agreement with the half-height width of the peaks in the experimental profile has been obtained for $L_a = L_b$ = 10 nm and L_c = 8 nm.

2.5. Energy Calculation Methods and Shape of Cavities. Energy calculations were carried out by using the Compass[16] force field within the *Open Force Field* module of *Cerius*[2] by the smart minimizer method with standard convergence. The starting conformation of the s-PS polymer chains was that found by molecular mechanics calculations reported in the literature.[17]

The shape of the cavities has been determined with the *Free Volume* module of *Cerius*[2] by calculating the region of the structure accessible to a probe species (with a radius of 0.1 nm) diffusing into the model from the exterior.

3. Results and Discussion

3.1. Additional Analysis on the Crystal Structure of the ε Form of s-PS. The X-ray fiber diffraction pattern of a uniaxially oriented sample of s-PS in the crystalline ε form and the relative intensity profile read along the equatorial line are reported in Figure 1. Figure 2 reports the X-ray diffraction pattern of an unoriented sample.

As for the specimen presented in ref 4b, both oriented and unoriented samples of Figures 1 and 2 show the presence of a minor amount of γ form, as revealed by the broad shoulder at $2\theta_{CuK\alpha}$ between 9° and 11° (indicated by the arrows in the profile of Figure 1(B) and in Figure 2), corresponding to the two strongest reflections of γ form, that alter the intensity and the shape of the peak at 2θ = 8.1° of the ε form. As far as the other reflections (both equatorial and on the layer lines) attributable to the γ form, it must be noted that these reflections are not directly detectable, even in the X-ray fiber diffraction pattern, since they are always overlapped with those of the ε form (the only exception is a very weak equatorial reflection at $2\theta \approx 19°$).

In order to estimate the intensity of the reflections of ε form, the contribution to the diffraction intensity of the γ form has been subtracted in the X-ray diffraction profiles of the oriented sample by a deconvolution procedure that has allowed establishing the intensity of the two most intense reflections of the γ form at 2θ = 9.2° and 10.3°. Successively, the intensities of the reflections belonging to the γ form at 2θ = 13.9°, 15.4°, 18.9°, 20.8°, 22.7°, and 23.8° were fixed according to the intensity ratios derived from the experimental profile presented in the inset of Figure 3 relative to a typical equatorial profile of a γ form sample. For the layer line reflections, the contributions to the diffraction intensities due to the γ form reflections centered at 16.0°,

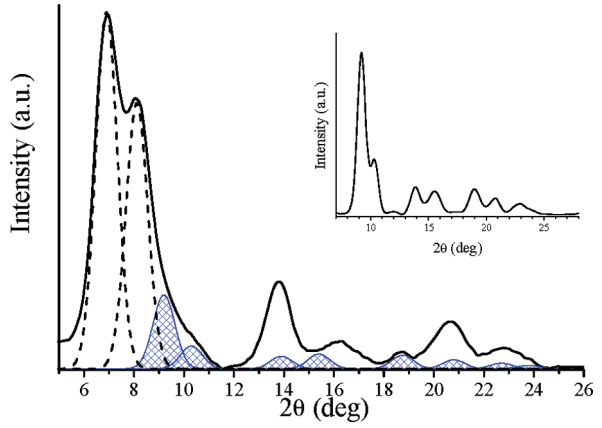

Figure 3. Evaluation of the contribution of the γ form (blue cross-filled peaks) in the equatorial intensity profile (black solid line) of the X-ray diffraction pattern of the s-PS ε form after subtraction of the amorphous and background contribution as shown in Figure 1B. The intensities of the reflections up to $2\theta \approx 12°$ were evaluated by a deconvolution procedure while those of the others were imposed according to the experimental ratios as obtained from a typical equatorial intensity profile of the s-PS γ form, after subtraction of the amorphous and background contribution (shown in the inset).

Table 1. Diffraction Angles ($2\theta_{obsd}$), Bragg Distances (d_{obsd}), and Intensities (I_{obsd}) in Arbitrary Units of the Reflections Observed on the Layer Lines (l) in the X-ray Fiber Diffraction Pattern of the Nanoporous ε Form of s-PS of Figure 1 after Subtraction of the Contributions of Amorphous, Background, and γ Form

l	$2\theta_{obsd}$ (deg)	d_{obsd} (nm)	I_{obsd}
0	6.9	1.28	11 739
0	8.1	1.09	8616
0	13.8	0.64	2546
0	16.4	0.54	778
0	20.4	0.435	1466
0	22.3	0.40	988
1	13.2	0.67	5980
1	16.1	0.55	66 740
1	20.2	0.44	38 516
1	23.2	0.38	9348
2	24.6	0.36	5200
2	28.0	0.32	9890
2	34.7	0.26	772

20.0°, and 23.6° for the first layer line and centered at 24.3°, 28.0°, and 34.6° for the second layer line were approximately evaluated and subtracted. The resulting intensities are reported in Table 1.

The experimental data reported in Table 1 can be well interpreted by the orthorhombic unit cell (with axes a = 1.62 nm, b = 2.20 nm, and c = 0.79 nm) and the space group *Pbcn* proposed in ref 4b. Consequently the minimum energy model proposed in that paper (whose fractional coordinates are reported in Table 2) are confirmed. On the basis of the intensity data reported in Table 1, the discrepancy factor between experimental and calculated structure factors according to this model is 0.16. The comparison between experimental and calculated structure factors is reported in Table 3.

An improvement of the agreement between experimental and calculated structure factors, respecting the constraints imposed by the symmetry, may be obtained by shifting the chains along the b axis. This shift produces, however, the shortening of some distances between non bonded carbon atoms belonging to neighboring chains. A compromise (for which R is lowered to 0.14 and the shortest distances between non bonded carbons belonging to neighboring chains are 0.35 nm) is obtained for a shift of +0.01 nm with respect to the minimum energy model. However, we think that this improvement of the agreement is not enough significant to justify a change in the structural model already proposed by some of us in ref 4b.

Table 2. Fractional Coordinates of the Atoms of the Asymmetric Unit of the Model of Minimum Energy for the Nanoporous ε Form of s-PS According to the Space Group *Pbcn*[a]

	x/a	y/b	z/c	o.f.[b]
C1	−0.006	0.196	0.497	1
C2	−0.056	0.158	0.368	1
C3	0.000	0.121	0.250	0.5
C4	*−0.113*	0.113	0.457	1
C5	*−0.084*	0.070	0.571	1
C6	*−0.136*	0.028	0.646	1
C7	*−0.220*	0.028	0.606	1
C8	*−0.251*	0.071	0.493	1
C9	*−0.198*	0.113	0.420	1
C10	−0.056	0.231	0.632	1
C11	0.000	0.268	−0.250	0.5
C12	*−0.118*	0.273	0.549	1
C13	*−0.095*	0.322	0.450	1
C14	*−0.153*	0.362	0.380	1
C15	*−0.237*	0.352	0.409	1
C16	*−0.261*	0.302	0.505	1
C17	*−0.202*	0.264	0.574	1

[a] Carbon atoms belonging to phenyl rings are indicated in italics. Hydrogen atoms were included in the structure factors calculation, but they are omitted in this table for simplicity. [b] Occupancy factor.

A further confirmation of the correctness of the model is given in Figure 4 where the calculated X-ray powder diffraction profile is compared to the experimental X-ray powder diffraction pattern, after subtraction of the amorphous and γ form contributions. A fairly good agreement is apparent.

A schematic representation of the model of minimum energy already presented in ref 4b, useful in the subsequent discussion of the cocrystal structure, is shown in Figure 5. The represented channel-shaped cavities correspond to the free volume available to guest molecules. The channel diameter has been evaluated in the range 0.45−0.50 nm.

3.2. s-PS/NA ε Clathrate: Crystal Structure Determination. The X-ray fiber diffraction pattern of a uniaxially oriented sample of a s-PS ε cocrystalline phase with NA and the relative intensity profile read along the equatorial line are reported in Figure 6. Figure 7 reports the X-ray diffraction pattern of an unoriented sample.

Also in this case, as for the nanoporous ε form, both patterns of Figures 6 and 7 clearly show that the samples contain a minor amount γ form. As for the fiber diffraction pattern, a procedure analogous to that applied in the case of the ε form has been performed for the equatorial reflections, in order to eliminate the γ form contribution to the reflections, as shown in Figure 8. No correction for the γ form contribution has been done for the layer line reflections. The resulting experimental data are reported in Table 4.

The experimental data reported in Table 4 are in agreement with the orthorhombic unit cell with axes a = 1.62 nm, b = 2.20 nm, and c = 0.79 nm and the space group *Pbcn* proposed for the nanoporous ε form. This indicates that crystal packing of the chains in the clathrate form remains substantially unaltered.

As we have already pointed out, the crystal structure of the s-PS ε form is characterized by the presence of channel shaped cavities passing the unit cell from side to side. It is worth noting that since there are no stoichiometric requirements to be fulfilled, the continuous nature of the channels could allow stacking of a variable number of guest molecules

Table 3. Comparison between Observed Structure Factors (F_{obsd}), Evaluated from the Intensities Reported in Table 1, and Calculated Structure Factors (F_{calcd}) for the Model of s-PS ε Form, Whose Fractional Coordinates Are Reported in Table 2[a]

hkl	d_{obsd} (nm)	d_{calcd} (nm)	F_{obsd}	F_{calcd}	
110	1.28	1.31	191	208	
020	1.09	1.10	177	153	
200		0.81		51	
130	0.64	0.67	126	20	142
220		0.65		140	
040	0.54	0.55	76	15	20
310		0.53		13	
330	0.44	0.44	118	163	165
150		0.43		27	
400	0.40	0.41	101	75	101
420		0.38		68	
530		0.30		66	
600		0.27		70	
550		0.26		48	
111	0.67	0.68	65	2	10
021		0.64		9	
211	0.55	0.55	282	272	299
131		0.51		102	
221		0.50		70	
041	0.44	0.45	260	39	268
231		0.45		52	
311		0.44		28	
141		0.44		259	
321		0.41		50	
331	0.38	0.38	142	15	172
151		0.37		171	
341		0.35		48	
421		0.34		47	
061		0.33		42	
531		0.28		44	
022	0.36	0.37	147	61	158
122		0.36		35	
202		0.36		118	
212		0.35		79	
042	0.32	0.32	277	17	245
232		0.32		43	
302		0.32		18	
312		0.32		9	
142		0.32		240	
162	0.26	0.27	100	57	121
432		0.26		7	
352		0.26		92	
262		0.26		52	

[a] The Bragg distances, observed in the X-ray fiber diffraction pattern reported in Figure 1 and calculated for the proposed orthorhombic unit cell (a = 1.62 nm, b = 2.20 nm, c = 0.79 nm), are also shown. Reflections not observed with F_{calcd} less than 40 have not been reported.

per monomer unit, whose maximum value depends only on their van der Waals encumbrance. For this reason in this type of cavities also guest molecules with molecular axis longer than the s-PS chain axis periodicity can be hosted with it parallel to the polymer chain axis, as already pointed out by IR measurements.[4a] In these cases, as for the guest

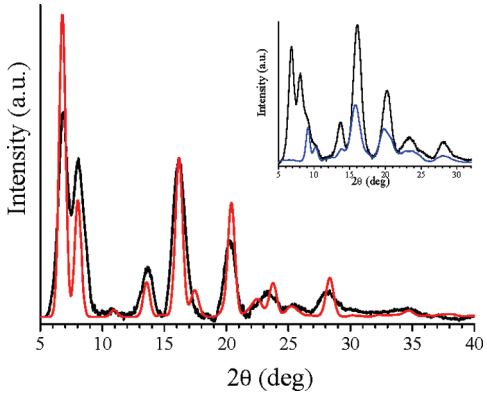

Figure 4. Comparison between the experimental X-ray powder diffraction pattern (black solid line) of the s-PS ε form after subtraction of the amorphous halo (Figure 2) and of the contribution of the γ form with the calculated one (red solid line) according to the structural model proposed in Figure 5. The inset shows the contribution of the γ form (in blue), subtracted to diffraction pattern of the prevailingly ε form sample.

molecules, the c periodicity of the ε form will be necessary lost.

It is worth noting that if in the lattice the chains are arranged according the space group *Pbcn*, the cavities that are delimited by them will possess the symmetries descending from that space group. Consequently, guest molecules can arrange themselves in different regions of the channels according to different but energetically equivalent ways related by these symmetry elements. For this reason, it can be expected that, at least in the equatorial projection, the structure can be assumed to be periodic with the symmetry required by the *Pbcn* space group. Consequently, as described in the next section, we have evaluated a discrepancy factor with the data derived from the fiber diffraction pattern only for the equatorial reflections by imposing a *Pbcn* symmetry. An evaluation of the agreement between experimental and calculated data on the whole spectrum has been performed only for the unoriented diffraction pattern. In this case we have described the model in the *P*1 symmetry using a "supercell" with the same a and b axis reported before but with a c axis that is a multiple of the chain repetition period and chosen in such a way to obtain the smallest cell with the maximum filling of the channel expressed by a integer number of guests.

In the case of the NA (whose van der Waals encumbrance along its main molecular axis is ≈0.93 nm), in the hypothesis that guests will be arranged with their axis exactly parallel to the c axis, the "supercell" satisfying the conditions reported before has a repetition period of 3.95 nm (five times that of the nanoporous ε form). In this "supercell" in each channel a maximum of four guest NA molecules can be hosted.

The placement of the guest molecules in the channels has been found through molecular mechanics calculations. In this analysis we used the before described "supercell", in which polymer helices were fixed according the minimum energy situation found for the *Pbcn* symmetry. In a first step, we have analyzed the arrangement of a single molecule in each channel. Then we have filled the channels with the maximum number (four) of guest molecules.

In the first case, we found several arrangements of the single guest molecule characterized by a very similar packing energy (apart from those related by the symmetry of the channels as previously discussed). It must be noted that in all these modes there is a wide degree of freedom for the position of the molecule along the channel axis while guest's main

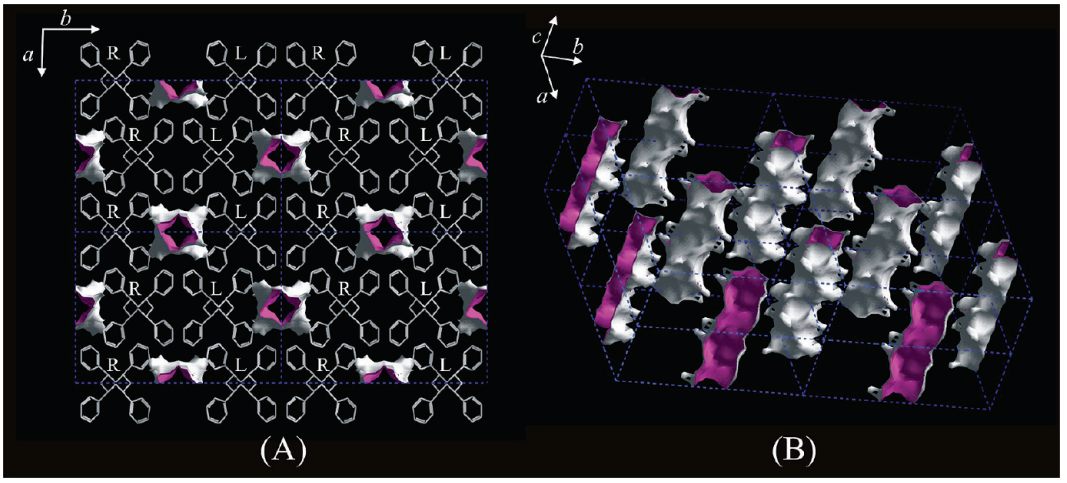

Figure 5. Packing model of the nanoporous ε form of s-PS in the projections along c (A) and in a tilted projection (B). The shape of the channels where guest molecules can be hosted is also represented. The internal face of the channels is reported in magenta while the external one (toward the chains) is reported in white. In part B, only the portion of the channels passing through eight neighboring cells are shown, while the polymer helices are omitted. R = right handed and L = left handed helical chains.

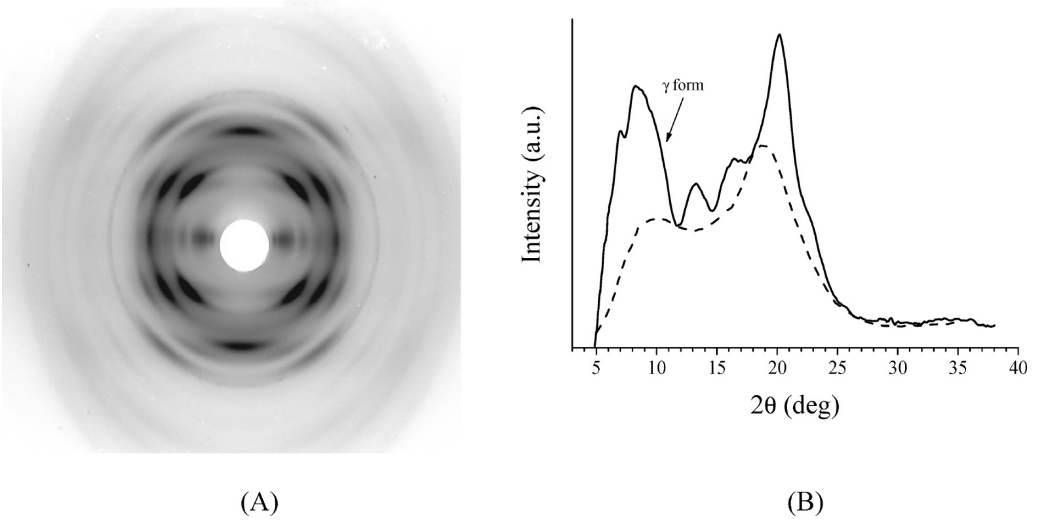

Figure 6. (A) X-ray diffraction pattern of an oriented sample of the s-PS/NA ε clathrate form. Fiber axis is vertical. In the corresponding equatorial intensity profile (B), the arrow indicates the position of the shoulder attributable to the presence of some amount of the γ polymorph. In part B, the amorphous and background contribution is indicated with a dashed line.

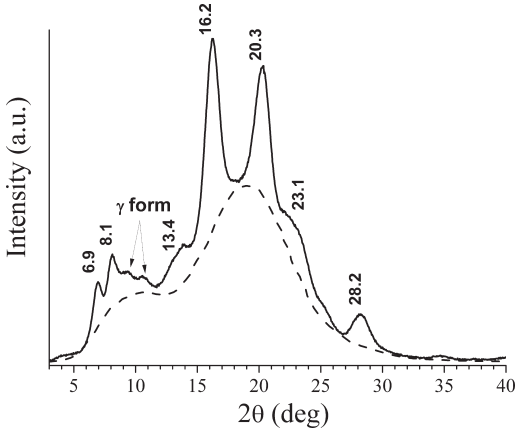

Figure 7. X-ray diffraction pattern of an unoriented sample of the s-PS/NA ε clathrate form. The amorphous and background contribution is indicated by a dashed line. The arrows indicate the positions of the reflections directly attributable to the presence in the sample of a minor amount of γ form.

molecular plane always forms with the *bc* plane an angle of nearly ±20° and its dipole is almost parallel to the chain axis.

The research of models of minimum energy imposing a maximum filling of the used "supercell" shows that due to the polarity of the guest, the packing energy varies if the nearest guests are arranged with parallel or opposite relative orientation. In particular, the minimum energy situation is obtained if guests are stacked in the channel all with the same relative dipole orientation (as in the case shown in Figures 9 and 10). If errors in the relative guest orientation are introduced in the same channel, the energy can increase up to nearly 4 kcal/mol of NA. The calculated energy, on the contrary, does not depend on the relative orientations of NA molecules in different channels. We have limited our analysis to models in which guest molecules have their dipole all with the same relative orientation. This analysis has shown that the guests are not uniformly distributed in the channel but arranged in "couples" in which successive molecules are linked by hydrogen bonds (between the NO_2 and NH_2 group) analogously to what has been found for the crystal structure of the NA, where the molecules are organized in

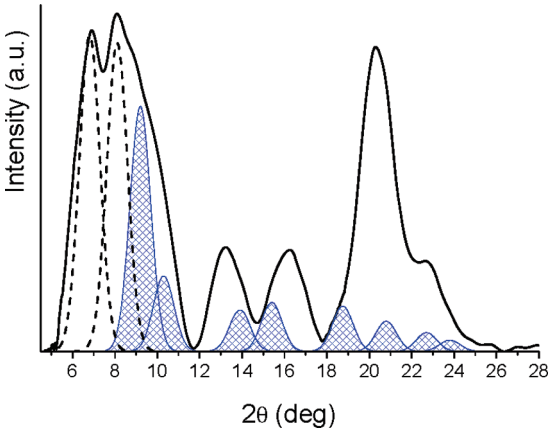

Figure 8. Evaluation of the contribution of the γ form (blue cross-filled peaks) in the equatorial intensity profile (black solid line) of the X-ray diffraction pattern of the s-PS/NA ε clathrate reported in Figure 6B after subtraction of the amorphous and background. The intensities of the reflections up to $2\theta \approx 12°$ were evaluated by a deconvolution procedure while those of the others were imposed according to the experimental ratios as obtained from a typical equatorial intensity profile of the s-PS γ form (see the inset of Figure 3), after subtraction of the amorphous and background contribution.

Table 4. Diffraction Angles ($2\theta_o$), Bragg Distances (d_{obsd}) and Intensities (I_{obsd}) in Arbitrary Units of the Reflections Observed on the Layer Lines (ℓ) in the X-ray Fiber Diffraction Pattern of the s-PS/NA ε Clathrate Form of Figure 6 After Subtraction of the Amorphous and Background Contribution. Only for the Equatorial Reflections the Contribution of the γ Form Shown in Figure 8 Has Been Subtracted

ℓ	$2\theta_{obsd}$ (deg)	d_{obsd} (nm)	I_{obsd}
0	6.9	1.28	6596
0	8.1	1.09	6251
0	13.2	0.67	1929
0	16.3	0.54	2200
0	20.2	0.44	8386
0	23.0	0.39	2176
1	13.10	0.68	527
1	15.95	0.56	6565
1	19.90	0.45	2857
1	23.00	0.39	771
2	24.60	0.36	1236
2	28.00	0.32	1801
2	34.60	0.26	71

row in which are all linked together by the formation of hydrogen bonds.[18] The fact that our calculations do not foresee a continuous enchainment of the guest molecules could be due to the fine structure of the channel. It is worth noting that the formation of the couples does not alter the orientation of the planes of the single molecules in respect to the *bc* plane we have described before. A representative model of minimum energy is that shown in Figure 9.[19]

A more detailed representation of the accommodation of the guest in the channels according the model of Figure 9 highlighting also the shape of the channels of the nanoporous ε form, is reported in Figure 10. From the figure it is apparent that the shape of the channel is not cylindrical but it presents a fine structure that induces the NA molecules to present their dipole nearly parallel to the polymer chain axis and their molecular plane nearly parallel to the *bc* plane.

3.3. Structure Factors Calculations. On the basis of the described model we have evaluated the agreement between experimental and calculated structure factor separately using the data obtainable from the equatorial layer line of the

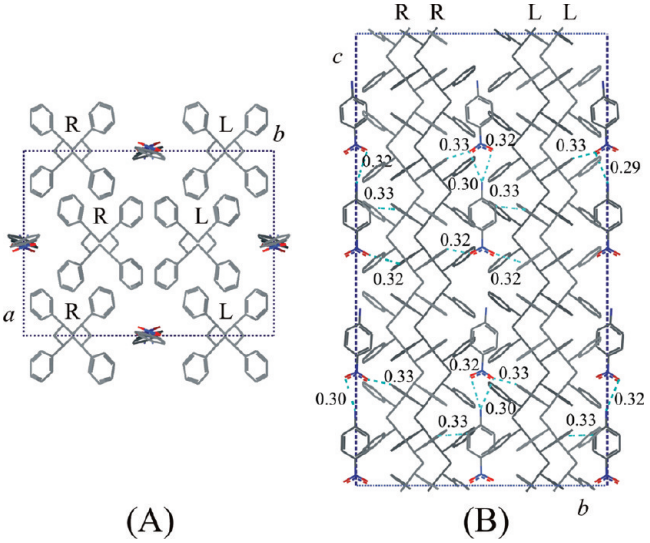

Figure 9. Packing model for the crystal structure of s-PS/NA ε cocrystalline form corresponding to one of the possible situations of minimum energy found imposing a maximum filling of the orthorhombic unit cell with constants $a = 1.62$ nm, $b = 2.20$ nm, $c = 3.95$ nm. (A) projection along *c* and (B) projection along *a*. Nonbonded distances (shorter than 0.34 nm) are reported in nm. R = right handed and L = left handed helical chains.

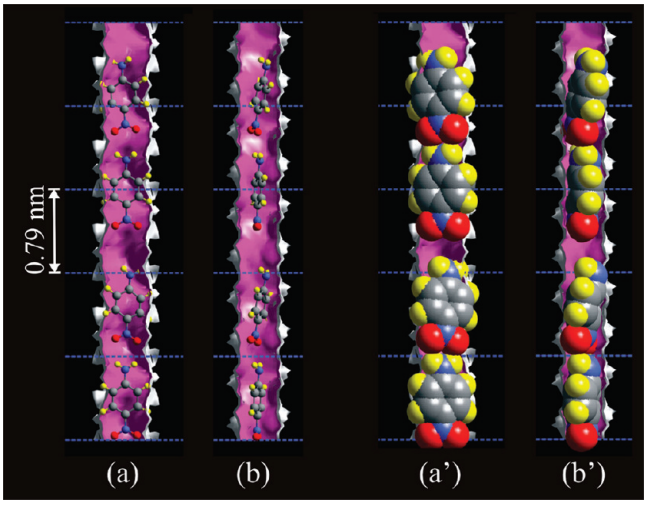

Figure 10. Schematic representation of some of the possible minimum energy arrangements of the NA guest molecules in the channels of the s-PS ε cocrystals found by molecular mechanics calculations. (a, a′) view of a cavity along the *a* axis. (b, b′) view of a cavity along the *b* axis. In parts a′ and b′, guest molecules are represented with their van der Waals steric hindrance. The chain repetition period is indicated by the dashed lines.

fiber diffraction pattern shown in Figure 6 and the X-ray diffraction pattern of an unoriented sample shown in Figure 7.

3.3.1. Fiber Diffraction Pattern. Structure factors were only calculated for the equatorial reflections in the space group *Pbcn* using the unit cell of the ε form ($a = 1.62$ nm, $b = 2.20$ nm, $c = 0.79$ nm). The asymmetric unit is constituted by half polymer helix (two subsequent repeating units) and one of the guest molecules of the model reported in Figure 9. The fractional coordinates of the guest molecule are reported in Table 5. An occupancy factor equal to $^1/_4k$, with $0 < k < 0.8$ ($k = 0.8$ nearly corresponding to the maximum occupancy) has been attributed to the coordinates of the guest. The best agreement between experimental and calculated structure

Table 5. Fractional Coordinates of the Atoms of the *p*-Nitroaniline Guest Molecule in the Model for the Crystal Structure of s-PS/NA ε Co-Crystalline Form Reported in Figure 9 with Constants a = 1.62 nm, b = 2.20 nm, and c = 3.95 nm According to the Space Group *Pbcn*[a]

	x/a	y/b	Z/c	o.f.[b]
C1	−0.005	0.500	0.367	0.125
C2	−0.020	0.552	0.462	0.125
C3	−0.008	0.551	0.636	0.125
C4	0.018	0.498	0.720	0.125
C5	0.033	0.446	0.623	0.125
C6	0.023	0.447	0.448	0.125
N1	−0.017	0.500	0.185	0.125
N2	0.031	0.498	0.895	0.125
O1	−0.007	0.452	0.110	0.125
O2	−0.036	0.547	0.118	0.125

[a] The fractional coordinates of the atoms of the polymer chain are those reported in Table 2. Hydrogen atoms were included in the structure factors calculation, but they are omitted in this table for simplicity. [b] Occupancy factor.

Table 6. Comparison between Observed Equatorial Structure Factors (F_{obsd}), Evaluated from the Intensities Observed in the X-ray Fiber Diffraction Pattern Shown in Figure 6, and Calculated Ones for the Model of s-PS/NA ε Clathrate Reported in Figure 9 Assuming a *Pbcn* Symmetry[a]

hkl	d_{obsd} (nm)	d_{calcd} (nm)	F_{obsd}	F_{calcd}	
110	1.28	1.31	111	114	
020	1.09	1.10	117	95	
130	0.67	0.67	83	82	106
220		0.65		67	
040	0.54	0.55	99	15	87
310		0.53		86	
240	0.44	0.46	216	53	224
330		0.44		211	
150		0.43		50	
400	0.39	0.41	118	117	119
420		0.38		17	
440		0.33		43	
530		0.30		96	
600		0.27		47	

[a] The Bragg distances, observed in the X-ray fiber diffraction pattern reported in Figure 6 and calculated for the orthorhombic unit cell with a = 1.62 nm, b = 2.20 nm, and c = 0.79 nm, are also shown. Reflections not observed with F_{calcd} less than 40 have not been reported.

factor is obtainable for k = 0.5. This corresponds to a guest content in the cocrystalline phase of 5.9 wt %.

The comparison between experimental and calculated structure factor is shown in Table 6. The discrepancy factor is 0.09. The agreement remains practically unchanged if different models with opposite guest dipole orientation in adjacent channels are considered.

3.3.2. Powder Diffraction Pattern. In this case, the calculated X-ray powder diffraction pattern has been generated for the model reported in Figure 9 obtained using *P*1 symmetry and a supercell with a = 1.62 nm, b = 2.20 nm, c = 3.95 nm. The fractional coordinates of the guests are reported as Supporting Information. The agreement with the experimental diffraction pattern has been optimized by changing the occupancy factor of the guest molecules. The best agreement (see Figure 11) is obtained considering an occupancy factor of 0.8 with reference to the model of Figure 9. It is apparent that the agreement with the experimental data is fairly good. The agreement remains practically unchanged if different models with opposite guest dipole orientation in adjacent channels are considered.

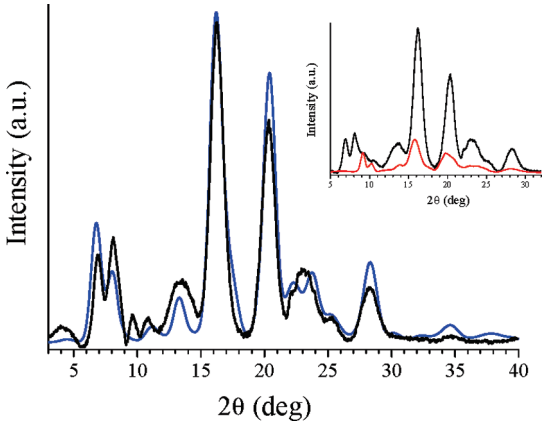

Figure 11. Comparison between the experimental (black line) X-ray powder diffraction pattern for the s-PS/NA ε clathrate form, after the subtraction of the amorphous and the γ form contributions, with the calculated one (blue line) according to the structural model of Figure 9. In the inset the contribution of the γ form (in red) subtracted to the s-PS/NA ε clathrate form diffraction pattern is shown.

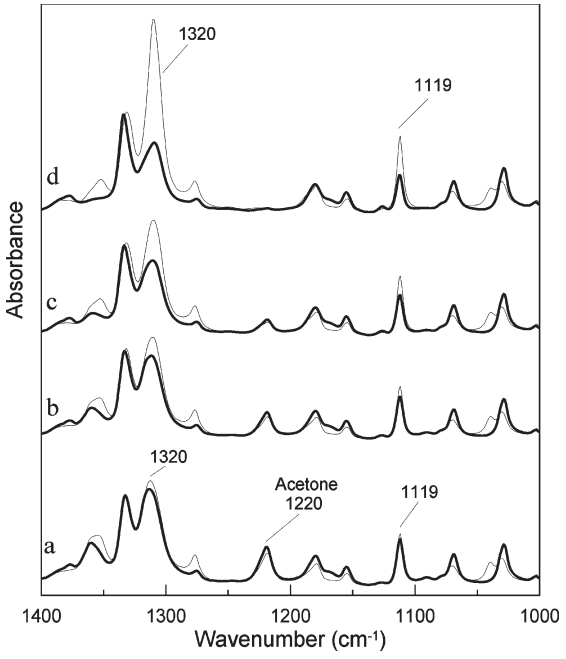

Figure 12. FTIR spectra in the wavenumber range 1400−1000 cm^{-1} taken with the polarization plane parallel (thin line) and perpendicular (thick line) to the draw direction for an uniaxially stretched ε film treated with a solution of acetone/*p*-nitroaniline during the progressive desorption of acetone: t_{des} = 0 (a), t_{des} = 45 min (b), t_{des} = 6 h (c), and t_{des} = 70 h (d).

3.4. FTIR Spectra of the s-PS/NA ε Clathrate. *3.4.1. Peak Dichroism: NA Orientation in the ε Clathrate Phase.* As already reported in previous papers,[4a,20] s-PS cocrystals with polar guests are easily obtained by treatments of δ, ε, or cocrystalline s-PS samples with concentrated solutions of these guests in suitable volatile carrier solvents such as acetone or acetonitrile. In Figure 12 are reported the polarized FTIR spectra of an uniaxially stretched ε-form film treated with an acetone solution saturated with *p*-nitroaniline, as collected during the progressive desorption of acetone.

We can observe that immediately after removal of the film from the solution, the dichroism of all NA peaks (at 1119 and

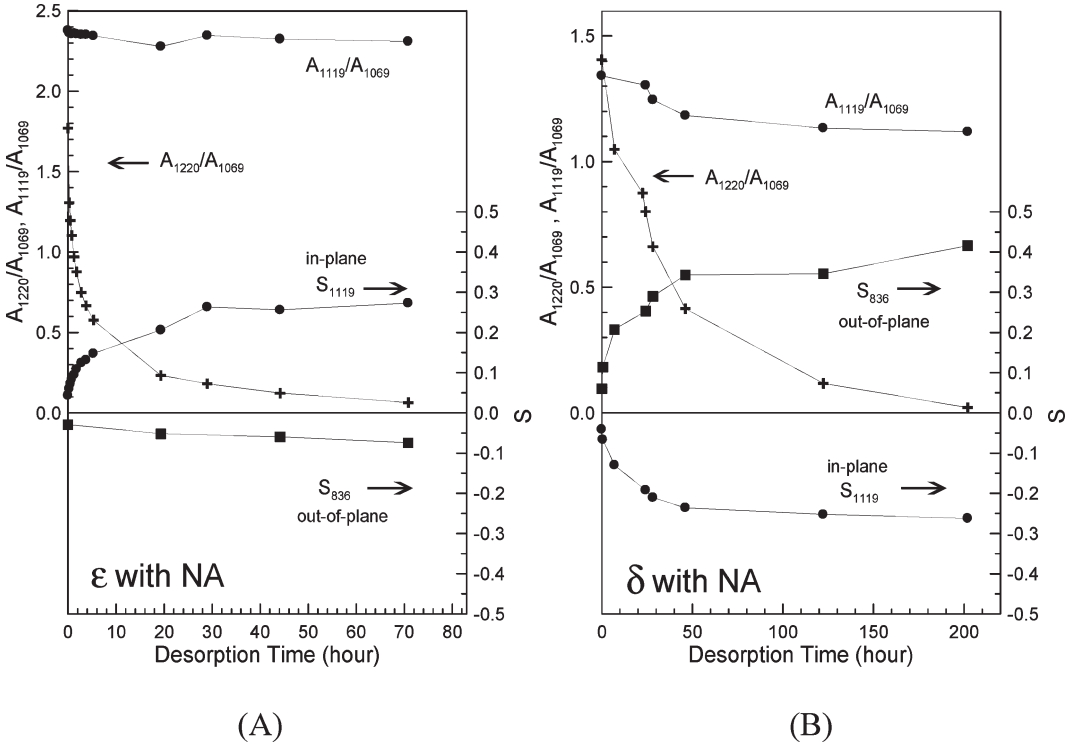

Figure 13. Absorbance of the acetone peak at 1220 cm^{-1} and NA peak at 1119 cm^{-1} (left scale) and of the linear dichroism of NA peaks (right scale) at 836 cm^{-1} (out-of-plane) and 1119 cm^{-1} (in plane) versus time for ε (A) and δ (B, data by Daniel et al.[19]) clathrate samples with NA.

1320 cm^{-1}) is low indicating (curve a) that most NA molecules are unoriented and hence located in the amorphous phase of the film. Then, during the spontaneous acetone desorption, the dichroism of NA peaks increases (curves b−d). Hence, as a consequence of acetone desorption, NA molecules migrate from the amorphous phase to the ε nanoporous crystalline phase.

This phenomenon is more clearly shown in Figure 13A where the acetone content (as evaluated by the absorbance of the peak at 1220 cm^{-1}), the NA content (as evaluated from the absorbance of the peak at 1119 cm^{-1}) and the order parameter of two NA peaks (out of plane at 836 cm^{-1} and in plane peak at 1119 cm^{-1})[21] are reported versus the desorption time. For the sake of comparison, results obtained for the δ clathrate sample with NA are also reported in Figure 13B (data by Daniel et al.[20]).

We can observe that for both δ and ε samples the dichroism of their NA peaks increases with the acetone desorption. However, it is clearly apparent that the dichroism sign of NA peaks depends on the host crystalline phase. In particular, for the film with the δ phase, the dichroism of the out-of plane peak at 836 cm^{-1} ((γ (CH-17b), symmetry b_1)[21] becomes markedly positive while the dichroism of the in-plane plane peak at 1119 cm^{-1} ((ν(7a, ph-NO_2) + ν(ph-1), symmetry a_1)[21] becomes negative (Figure 13B). Conversely, for the film with the ε phase, the dichroism of 836 and 1119 cm^{-1} peaks becomes negative and positive, respectively (Figure 13A). These data can be explained by a different orientation of the NA molecules in the two cocrystalline phases: in δ clathrate, NA molecules assume an orientation of their dipole moments nearly perpendicular to the chain axis[2e] while in ε clathrates, NA molecules tend to assume an orientation of the molecular dipole roughly parallel to the chain axis.

These results are in qualitative agreement with the NA guest orientation as established in ref 2e and in previous sections of the present paper, for the δ and ε clathrates, respectively.

3.4.2. Peak Shift: NA Content and Interactions in the ε Clathrate Phase. The shape and the position of N−H stretching peaks of NA molecules at ca. 3400 cm^{-1} (($\nu_s(NH_2)$, symmetry a_1)[21] and 3500 cm^{-1}(($\nu_{as}(NH_2)$, symmetry a_2)[21] allow to evaluate the relative amount of NA in the amorphous and the crystalline phases. In fact, the position of these stretching peaks is strongly dependent on the possible formation of hydrogen bonds. For instance, these peaks for NA molecules in the solid crystalline are located at 3360−3363 cm^{-1} and 3481−3485 cm^{-1}, while for fully isolated NA molecules are located at ca. 3510 and 3410 cm^{-1}, respectively.[22]

In Figure 14A are compared the FTIR spectra in the N−H stretching modes area of pure crystalline NA and of ε/NA and δ/NA film samples, as collected immediately after removal from the acetone solution (thin line) and after complete desorption of acetone (thick line). For the crystalline NA the spectrum displays, in addition to the two strong absorption bands at 3483 ($\nu_{as}(NH_2)$) and 3361 cm^{-1} ($\nu_s(NH_2)$), two other bands with lower absorbances at 3242 and 3220 cm^{-1}. These two bands are due to NH_2 groups involved in a hydrogen bonding system.[22]

We can observe that for the δ/NA clathrate sample a large band centered at 3240 cm^{-1} is present, before acetone removal. We can attribute this band to hydrogen bonding between the NH_2 and NO_2 group of NA molecules included in the amorphous. Then when all the NA molecules are included in the crystalline δ form, this band vanishes. The absence of hydrogen bonding is due to the inclusion of the NA molecules in the isolated cavities of the δ form.

For the ε/NA sample, we can observe that the absorbance of the two bands due to hydrogen bonding decreases after inclusion of NA molecules in the ε crystalline phase. However, unlike for the δ/NA sample, the bands do not vanish completely and two peaks located at 3243 and 3215 cm^{-1} are still present. This result suggests that some NA molecules

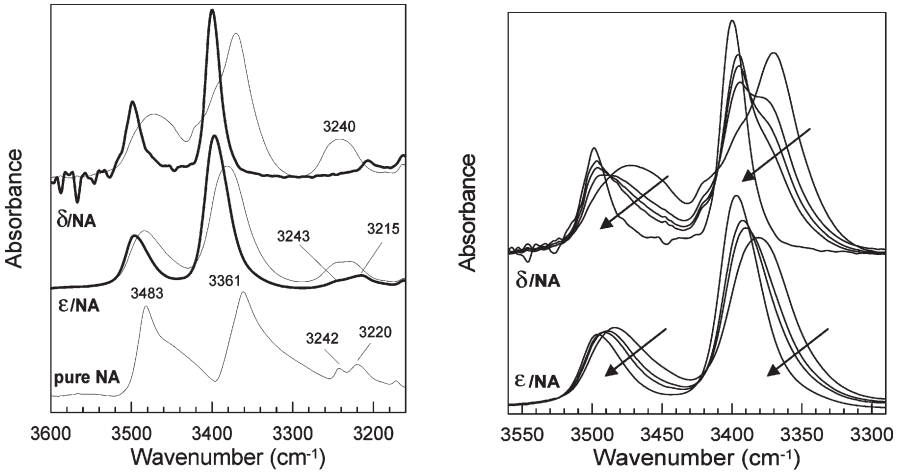

Figure 14. (A) FTIR spectra in the wavenumber range 3600−3160 cm^{-1} of pure crystalline NA and of ε/NA and δ/NA film samples collected immediately after removal from the acetone solution (thin line) and after complete desorption of acetone (thick line). (B) FTIR spectra in the wavenumber range 3560−3290 cm^{-1} collected during the progressive acetone desorption for ε and δ form samples.

included in the channels of the ε cocrystals are still involved in hydrogen bonding.

It is worth adding that for the δ/NA clathrate sample, after acetone desorption, both N−H stretching peaks (at 3400 and 3500 cm^{-1}) become narrow and symmetric and their position is not far from that one observed for isolated NA molecules in suitable solvents such as chloroform.[22a,c] This indicates that most NA molecules, after acetone desorption, are located as isolated guests of the cocrystalline phase. As for the s-PS/NA ε clathrate sample, also after complete acetone desorption, NA peaks remain broader and asymmetric, maintaining a component at lower wavenumber, clearly confirming the maintenance of some guest−guest hydrogen bond. This N−H peak asymmetry has been confirmed for many s-PS/NA ε clathrate samples of different thickness and prepared from different NA solutions.

In Figure 14B are reported the FTIR spectra in the wavenumber range 3290−3560 cm^{-1} collected during the progressive migration of NA molecules from the amorphous phase to the ε phase and to the δ phase. In the assumption that the NH stretching peaks of the clathrate samples (after complete acetone removal) correspond to NA molecules being guest of the cocrystalline phases, the relative amount of NA molecules included in the crystalline phase and the amorphous phase of the ε/NA and δ/NA samples can be determined by spectral subtraction (see paragraph 2.3 of the Experimental Section).

Figure 15 reports the variation of the fraction of NA molecules included in the ε and δ crystalline phase during the acetone desorption. For the ε/NA sample we can observe that just after removal of the film from the acetone solution saturated with NA, ca. 40% of NA molecules are already included in the crystalline phase and after 70 h of acetone desorption almost 90% of the NA molecules are included in the ε/NA cocrystalline phase.

By applying this FTIR analysis to the uniaxially oriented s-PS/NA ε clathrate sample used for the crystal structure determination it was found that the total amount of NA molecules in the sample is ca. 5.5 wt %, and more than 98% of the NA molecules are included in the ε crystalline phase. This guest amount is a good agreement with that one evaluated in section 3.3.1 (5.9 wt %), by comparison between observed and calculated structure factors.

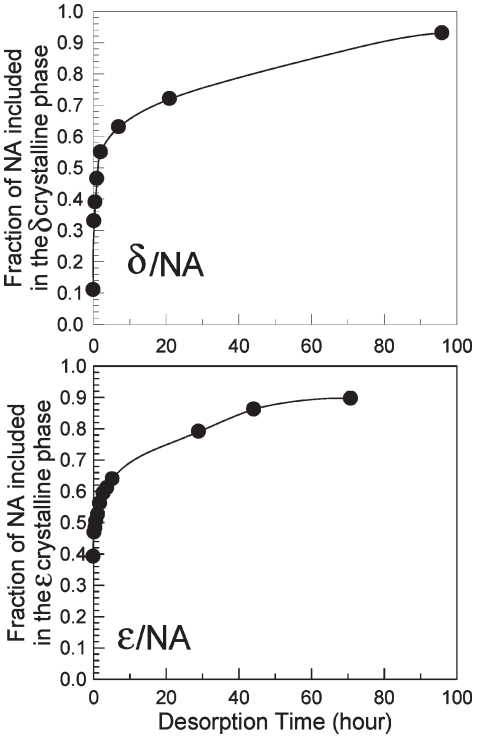

Figure 15. Variation of the fraction of NA molecules included in the ε (bottom) and the δ (up) crystalline phases, during the progressive desorption of acetone.

The fraction of NA guest molecules of the ε clathrate phase exhibiting hydrogen bonds, has been estimated by a comparison of the 3400 cm^{-1} peak of the δ and ε clathrates (thick lines in Figure 14A). In particular, it is assumed that the asymmetry of the ε clathrate peak (after complete solvent carrier desorption) is due to the formation of guest−guest hydrogen bonds into the channels. Then, on the basis of subtraction of the peaks of the δ clathrate (where all NA molecules are isolated),[2e] the fraction of NH_2 groups involved in hydrogen bonds has been evaluated in the range 25−35%. This indicates that the fraction of NA molecules involved in NH_2−NO_2 bonding in the channels of the ε/NA cocrystalline phase is in the range 50−70%. This result

qualitatively confirms the predictions of molecular mechanics calculations reported in the previous section, showing that NA molecules are not uniformly distributed in the channel but mainly arranged in "couples".

4. Conclusions

This contribution presents, for the first time, the detailed description of the crystalline structure of a channel type ε clathrate cocrystal of s-PS. The relevance of this structural study is also associated with the high polarity of the *p*-nitroaniline guest molecule, which makes its cocrystals possibly suitable for nonlinear optical and piezo-electric materials.

As a preliminary step to the cocrystal structure determination, we have performed a more quantitative analysis of the crystal structure of the nanoporous s-PS ε form. On the basis of powder and fiber spectra, the structural model exhibiting empty channels, parallel to the host helical chain axes, has been confirmed.

The diffraction data of the s-PS/NA ε clathrate are in agreement with the orthorhombic unit cell with axes $a = 1.62$ nm, $b = 2.20$ nm and $c = 0.79$ nm and the space group *Pbcn*, proposed for the nanoporous ε form indicating that the crystal packing of the chains in the clathrate form remains substantially unaltered. Since no stoichiometric requirements have to be fulfilled, the continuous nature of the channels allows stacking of a variable number of guest molecules per monomer unit, whose maximum value depends only on their van der Waals encumbrance.

The placement of the NA guest molecules in these channels has been found through molecular mechanics calculations and supported by structure factor comparison with diffraction data. We found several arrangements of the guest molecule characterized by similar packing energy and a high degree of freedom as for the guest position along the channel axis. However, for all these arrangements, the NA guest dipole is almost parallel to the chain axis while the NA main molecular plane forms with the *bc* plane an angle of nearly ±20°.

The *c* periodicity of the ε form is necessarily lost for the ε clathrate with NA, because of the parallel orientation of the NA guest with respect to the polymer chain axis and because the NA molecular axis (0.93 nm) is bigger than the chain axis periodicity (0.78 nm).

The reported molecular simulations also indicate that the minimum energy packing is obtained if guests are stacked in each channel all with a same relative dipole orientation and that the guests are not uniformly distributed in the channel but arranged in "couples", in which molecules are linked by hydrogen bonds (between the NO_2 and NH_2 group).

FTIR measurements have also given relevant information on the structure of the s-PS/NA ε clathrate. In particular, the linear dichroism is negative and positive for the out-of-plane and in-plane guest peaks, respectively. These data confirm that, in the ε clathrate, the NA guest molecules are oriented with their molecular dipole roughly parallel to the chain axis.

The shape and the position of N−H stretching peaks of NA molecules at ca. 3400 and 3500 cm^{-1} allow to evaluate the relative amount of NA in the amorphous and the crystalline phases. In particular, by applying this FTIR analysis to the uniaxially oriented s-PS/NA ε clathrate sample used for the crystal structure determination it was found that the total amount of NA molecules in the sample is ca. 5.5 wt % with most of the NA molecules included in the ε crystalline phase (in a good agreement with the guest amount of 5.9 wt % evaluated by the X-ray diffraction study).

For the ε clathrate phase, two bands due to hydrogen bonding are clearly present (at 3243 and 3215 cm^{-1}) and indicate that some NA molecules included in the channels of the ε cocrystals are still involved in hydrogen bonding. The maintenance of some guest−guest hydrogen bond in the channels of the ε clathrate is confirmed by the presence of broad and asymmetric N−H stretching peaks. In qualitative agreement with the predictions of molecular simulations, spectral subtraction procedures indicate that the fraction of NA guest molecules of the ε clathrate phase exhibiting hydrogen bonds is in the range 50−70%.

Acknowledgment. We thank Dr. Alexandra Albunia and Dr. Marco Della Mura of University of Salerno for useful discussions. Financial support of the "Ministero dell'Istruzione, dell'Università e della Ricerca" (PRIN2007), of "Regione Campania" (Legge 5) and of the Consortium INSTM (PRISMA 01/2007) is gratefully acknowledged.

Supporting Information Available: A table of the fractional coordinates of the *p*-nitroaniline guest molecules hosted in the orthorhombic "supercell" with $a = 1.62$ nm, $b = 2.20$ nm, $c = 3.95$ nm shown in Figure 9. This material is available free of charge via the Internet at http://pubs.acs.org.

References and Notes

(1) (a) Guerra, G.; Vitagliano, V. M.; De Rosa, C.; Petraccone, V.; Corradini, P. *Macromolecules* **1990**, *23*, 1539–1544. (b) Chatani, Y.; Shimane, Y.; Inoue, Y.; Inagaki, T.; Ishioka, T.; Ijitsu, T.; Yukinari, T. *Polymer* **1992**, *33*, 488–492. (c) Rizzo, P.; D'Aniello, C.; De Girolamo Del Mauro, A.; Guerra, G. *Macromolecules* **2007**, *40*, 9470–9474. (d) Milano, G.; Guerra, G. *Progr. Mater. Sci.* **2009**, *54*, 68–88. (e) Gowd, E. B.; Tashiro, K.; Ramesh, C. *Prog. Polym. Sci.* **2009**, *34*, 280–315.

(2) (a) Chatani, Y.; Shimane, Y.; Inagaki, T.; Ijitsu, T.; Yukinari, T.; Shikuma, H. *Polymer* **1993**, *34*, 1620–1624. (b) Chatani, Y.; Inagaki, T.; Shimane, Y.; Shikuma, H. *Polymer* **1993**, *34*, 4841–4845. (c) De Rosa, C.; Rizzo, P.; Ruiz De Ballesteros, O.; Petraccone, V.; Guerra, G. *Polymer* **1998**, *40*, 2103–2110. (d) Tarallo, O.; Petraccone, V. *Macromol. Chem. Phys.* **2004**, *205*, 1351–1360. (e) Tarallo, O.; Petraccone, V.; Daniel, C.; Guerra, G. *CrystEngComm* **2009**, *11*, 2381–2390.

(3) (a) Petraccone, V.; Tarallo, O.; Venditto, V.; Guerra, G. *Macromolecules* **2005**, *38*, 6965–6971. (b) Tarallo, O.; Petraccone, V.; Venditto, V.; Guerra, G. *Polymer* **2006**, *47*, 2402–2410.

(4) (a) Rizzo, P.; Daniel, C.; De Girolamo Del Mauro, A.; Guerra, G. *Chem. Mater.* **2007**, *19*, 3864–3866. (b) Petraccone, V.; Ruiz de Ballesteros, O.; Tarallo, O.; Rizzo, P.; Guerra, G. *Chem. Mater.* **2008**, *20*, 3663–3668.

(5) (a) De Rosa, C.; Guerra, G.; Petraccone, V.; Pirozzi, B. *Macromolecules* **1997**, *30*, 4147–4152. (b) Milano, G.; Venditto, V.; Guerra, G.; Cavallo, L.; Ciambelli, P.; Sannino, D. *Chem. Mater.* **2001**, *13*, 506–1511. (c) Gowd, E. B.; Shibayama, N.; Tashiro, K. *Macromolecules* **2006**, *39*, 8412–8418.

(6) (a) Daniel, C.; Deluca, M. D.; Guenet, J. M.; Brulet, A.; Menelle, A. *Polymer* **1996**, *37*, 1273–1280. (b) Rastogi, S.; Goossens, J. G. P.; Lemstra, P. J. *Macromolecules* **1998**, *31*, 2983–2998. (c) van Hooy-Corstjens, C. S. J.; Magusin, P. C. M. M.; Rastogi, S.; Lemstra, P. J. *Macromolecules* **2002**, *35*, 6630–6637. (d) Galdi, N.; Albunia, A. R.; Oliva, L.; Guerra, G. *Macromolecules* **2006**, *39*, 9171. (e) Malik, S.; Rochas, C.; Guenet, J. M. *Macromolecules* **2006**, *39*, 1000–1007.

(7) (a) Wübbenhorst, M.; van Turnhout, J.; Klap, G.; Jansen, J. C.; Quintel, A.; Hulliger, J. *IEEE Transactions on Dielectrics and Electrical Insulation* **2000**, *7*, 523–530. (b) Hertzsch, T.; Kluge, S.; Weber, E.; Budde, F.; Hulliger, J. *Adv. Mater.* **2001**, *13*, 1864–1867. (c) Gervais, C.; Hertzsch, T.; Hulliger, J. *J. Phys. Chem. B* **2005**, *109*, 7961–7968.

(8) (a) Rizzo, P.; Lamberti, M.; Albunia, A. R.; Ruiz de Ballesteros, O.; Guerra, G. *Macromolecules* **2002**, *35*, 5854–5860. (b) Rizzo, P.; Della Guardia, S. D.; Guerra, G. *Macromolecules* **2004**, *37*, 8043–8049. (c) Rizzo, P.; Spatola, A.; De Girolamo Del Mauro, A.; Guerra, G. *Macromolecules* **2005**, *38*, 10089–10094. (d) Albunia, A. R.; Rizzo, P.; Tarallo, O.; Petraccone, V.; Guerra, G. *Macromolecules* **2008**, *41*, 8632–8642.

(9) (a) Albunia, A. R.; Milano, G.; Venditto, V.; Guerra, G. *J. Am. Chem. Soc.* **2005**, *127*, 13114. (b) Uda, Y.; Kaneko, F.; Tanigaki, N.; Kawaguchi, T. *Adv. Mater.* **2005**, *17*, 1846. (c) Albunia, A. R.; Graf, R.; Grassi, A.; Guerra, G.; Spiess, H. W. *Macromolecules* **2009**, *42*, 4929–4931. (d) Albunia, A. R.; D'Aniello, C.; Guerra, G.; Gatteschi, D.; Mannini, M.; Sorace, L. *Chem. Mater.* **2009**, *21*, 4750–4752.

(10) Itagaki, H.; Sago, T.; Uematsu, M.; Yoshioka, G.; Correa, A.; Venditto, V.; Guerra, G. *Macromolecules* **2008**, *41*, 9156–9164.
(11) Albunia, A. R.; Rizzo, P.; Guerra, G. *Chem. Mater.* **2009**, *21*, 3370–3375.
(12) (a) de Candia, F.; Filho, A. R.; Vittoria, V. *Makromol. Chem. Rapid Commun.* **1991**, *12*, 295–299. (b) Petraccone, V.; Auriemma, F.; Dal Poggetto, F.; De Rosa, C.; Guerra, G.; Corradini, P. *Makromol. Chem.* **1993**, *194*, 1335–1345. (c) Auriemma, F.; Petraccone, V.; Dal Poggetto, F.; De Rosa, C.; Guerra, G.; Manfredi, C.; Corradini, P. *Macromolecules* **1993**, *26*, 3772–3777. (d) Montefusco, T.; Daniel, C.; Rizzo, P.; Musto, P.; Guerra, G. Submitted for publication in *Polym. Adv. Tech.*
(13) Albunia, A. R.; Musto, P.; Guerra, G. *Polymer* **2006**, *47*, 234–242.
(14) Torres, F. J.; Civalleri, B.; Meyer, A.; Musto, P.; Albunia, A. R.; Rizzo, P.; Guerra, G. *J. Phys. Chem. B* **2009**, *113*, 5059–5071.
(15) *International tables for X-ray crystallography* Vol. *4*, The Kynoch Press: Birmingham, England, 1974.
(16) Sun, H. *J. Phys. Chem. B* **1998**, *102*, 7338.
(17) Corradini, P.; Napolitano, R.; Pirozzi, B. *Eur. Polym. J.* **1990**, *26*, 157.
(18) Trueblood, K. N.; Goldish, E.; Donohue, J. *Acta Crystallogr.* **1961**, *14*, 1009.
(19) According to our calculations, the antiparallel orientation of NA chains between two cavities in a unit cell should be the most probable structure. Since the agreement between experimental and calculated structure factors remains practically unchanged if models with parallel or antiparallel guest dipole orientation in adjacent channels are considered, in Figure 9 and 10, we have chosen as representative a situation with parallel guests. We have been moved by the fact that the relevance of this structural study is also associated with the high polarity of the *p*-nitroaniline guest molecule, which makes its cocrystals possibly suitable for nonlinear optical and piezo-electric materials. So, the models of Figures 9 and 10 represent a "poled" situation, for which these properties are maximized.
(20) Daniel, C.; Galdi, N.; Montefusco, T.; Guerra, G. *Chem. Mater.* **2007**, *19*, 3302.
(21) (a) Vijama Kumar, D.; Ashok Babu, V.; Ramana Rao, G.; Pandey, G. C. *Vib. Spectrosc.* **1992**, *4*, 39. (b) Kozich, V.; Werncke, W.; Dreyer, J.; Brzezinka, K. W.; Rini, M.; Kummrow, A.; Elsaesser, T. *J. Chem. Phys.* **2002**, *117*, 719.
(22) (a) Marlow, F.; Demuth, D.; Stucky, G.; Schüth, F. *J. Phys. Chem.* **1995**, *99*, 1306. (b) Binder, G.; Scandella, L.; Kritzenberger, J.; Gobrecht, J.; Koegler, J. H.; Prins, R. *J. Phys. Chem. B.* **1997**, *101*, 483. (c) Kinski, I.; Daniels, P.; Deroche, C.; Marler, B.; Gies, H. *Microporous Mesoporous Mater.* **2002**, *56*, 11.